In Situ Formation of Efficient Cobalt-Based Water Oxidation Catalysts from Co2+ -Containing Tungstate and Molybdate Solutions

ARTICLE *in* CHEMISTRY - AN ASIAN JOURNAL · APRIL 2015

Impact Factor: 4.59 · DOI: 10.1002/asia.201500099 · Source: PubMed

6 AUTHORS, INCLUDING:

Biaobiao Zhang

KTH Royal Institute of Technology

12 PUBLICATIONS **187** CITATIONS

SEE PROFILE

Fei Li

George Mason University

37 PUBLICATIONS **352** CITATIONS

SEE PROFILE

ACES

DOI: 10.1002/asia.201500099

CHEMISTRY
AN ASIAN JOURNAL
Full Paper

Heterogeneous Catalysis

In Situ Formation of Efficient Cobalt-Based Water Oxidation Catalysts from Co^{2+}-Containing Tungstate and Molybdate Solutions

Biaobiao Zhang,[a] Xiujuan Wu,[a] Fei Li,*[a] Fengshou Yu,[a] Yong Wang,[a] and Licheng Sun[a, b]

Dedicated to Professor Mei Wang on the occasion of her 60th birthday

Abstract: Replacing rare and expensive noble-metal catalysts with inexpensive and earth-abundant ones is of great importance to split water either electrochemically or photoelectrochemically. In this study, two amorphous cobalt oxide catalysts (Co–W film and Co–Mo film) with high activity for electrocatalytic water oxidation were prepared by fast, simple electrodeposition from aqueous solutions of Na_2WO_4 and Na_2MoO_4 containing Co^{2+}. In solutions of Na_2WO_4 and Na_2MoO_4, sustained anodic current densities up to 1.45 and 0.95 mA cm^{-2} were obtained for Co–W film at 1.87 V versus a reversible hydrogen electrode (RHE) and Co–Mo film on fluorine-doped tin oxide (FTO) substrates at 1.85 V versus RHE. For the Co–W film, a much higher current density of 4.5 mA cm^{-2} was acquired by using a stainless-steel mesh as the electrode substrate. Significantly, in long-term electrolysis for 13 h, the Co–W film exhibited improved stability in cobalt-free buffer solution in comparison with the previously reported Co–Pi film.

Introduction

The exploitation of applicable sources of renewable and carbon-neutral energy, such as sunlight, is driven by ever-increasing worldwide energy requirements.[1] The production of hydrogen through electro- or photochemical water splitting is a promising approach to store solar energy in a chemical, stable form before further usage.[2–6] Electrochemical water oxidation, which forms molecular oxygen, protons, and electrons, plays an important role in electrochemical fuel production. However, a large overpotential is normally required to drive this reaction owing to the complexity of the $4H^+/4e^-$ process required for oxygen evolution.[7] There is thus a crucial need to design water oxidation anodes modified with efficient electrocatalysts with the criteria of high activity, long-term stability, and abundance of the materials used.[8,9]

To date, the most active electrocatalysts are those based on expensive metals, such as platinum,[10] IrO_x,[11] and RuO_x.[12] To replace traditional expensive electrocatalysts, electrocatalysts based on non-noble metals, such as iron,[13,14] cobalt,[15–18] nickel,[19–21] and copper,[22,23] have been explored. However, few of them showed both high activity and high stability under benign conditions. Recently, an amorphous cobalt oxide catalyst (Co–Pi) formed by electrodeposition from a phosphate buffer containing Co^{2+} was reported to efficiently catalyze the oxidation of water under benign conditions.[17] The robustness of Co–Pi benefits from a self-repairing mechanism in the presence of the Co^{2+} ion and a proton buffer solution. By using a similar method, amorphous cobalt oxides were fabricated by electrodeposition from other Co^{2+}-containing buffers, such as solutions of F^-, trifluoromethanesulfonamide ($TfNH_2$), BF_4^-, and HCO_3^-/CO_2 (Ci).[16,24,25] Among them, the Co–Ci catalyst is the only one that has shown long-term stability in controlled potential electrolysis (CPE) under cobalt-free conditions, which indicates the importance of the electrolyte on proton transfer and ion exchange at the interface between the aqueous solution and metal oxide.[25] To develop a more robust electrocatalyst, we report herein cobalt-based electrocatalysts prepared by electrodeposition from Co^{2+} in aqueous solutions of tungstate and molybdate. The new catalysts exhibited high activity and extraordinary stability in long-term electrolysis over 20 h in pure solutions of tungstate or molybdate at near-neutral pH; this makes them among the best electrocatalysts for water oxidation under benign conditions.

[a] *B. Zhang, Dr. X. Wu, Dr. F. Li, F. Yu, Y. Wang, Prof. L. Sun*
State Key Laboratory of Fine Chemicals
DUT-KTH Joint Education and Research Center on Molecular Devices
Dalian University of Technology (DUT)
116024 Dalian (P.R. China)
Fax: (+86) 411-84986245
E-mail: lifei@dlut.edu.cn

[b] *Prof. L. Sun*
Department of Chemistry
School of Chemical Science and Engineering
Royal Institute of Technology (KTH)
10044 Stockholm (Sweden)

Supporting information for this article is available on the WWW under http://dx.doi.org/10.1002/asia.201500099.

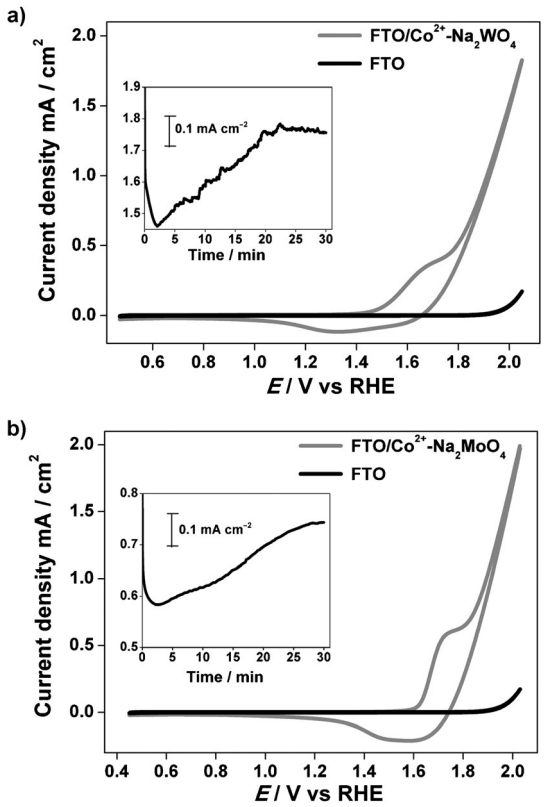

Figure 1. Cyclic voltammograms of FTO electrodes a) in 50 mM solutions of Na_2WO_4 at pH 8.0 with (gray) and without (black) the presence of $Co(NO_3)_2$ (2 mM); or b) in 60 mM solutions of Na_2MoO_4 at pH 7.6 with (gray) and without (black) the presence of $Co(NO_3)_2$ (2 mM). Scan rate: 100 mV s^{-1}; electrode area $A = 1$ cm^2.

Results and Discussion

Cyclic voltammograms (Figure 1 a) of $Co(NO_3)_2$ in a solution of Na_2WO_4 in a three-electrode setup with a fluorine-doped tin oxide (FTO) working electrode, a platinum counter electrode, and a reference electrode composed of an aqueous solution of Ag/AgCl containing KCl (3.5 M) exhibits an anodic wave at 1.67 V (versus the reversible hydrogen electrode (RHE)), which is attributed to the oxidation of Co^{II} to Co^{III}. A prominent catalytic wave occurs at 1.77 V followed by a broad weak reduction wave during the cathodic scan. Similar cyclic voltammetry (CV) behavior was observed for $Co(NO_3)_2$ in an aqueous solution of Na_2MoO_4, in which the oxidation of cobalt and the catalytic wave were observed at 1.75 and 1.83 V, respectively (Figure 1 b). Then, bulk electrolysis was carried out at 1.87 V for the Co–W film and 1.85 V for the Co–Mo film without stirring. The electrolyte was either a 50 mM aqueous solution of Na_2WO_4 containing 2 mM $Co(NO_3)_2$ or a 60 mM aqueous solution of Na_2MoO_4 containing 2 mM $Co(NO_3)_2$. In both cases, a layer of brown film formed on the FTO substrate in 30 min (denoted as Co–W film and Co–Mo film, respectively; Figure S1 in the Supporting Information). During electrolysis, the current densities rise to a plateau of 1.7 mA cm^{-2} for Na_2WO_4 and 0.7 mA cm^{-2} for Na_2MoO_4 (insets in Figure 1 a and b). Oxygen bubbles were concurrently observed, which was indicative of the in situ formation of oxygen-evolving catalysts (OEC). Control experiments showed that the catalytic activity did not depend on the source of the cobalt salt. Upon replacing $Co(NO_3)_2$ with $CoSO_4$ or $Co(CH_3CO_2)_2$, essentially the same catalytic performance was obtained. However, replacing Co^{2+} with other metal ions, such as Fe^{2+}, Cu^{2+}, Mn^{2+}, and Ni^{2+}, led to significantly reduced activities (Figure S2 in the Supporting Information).

The morphologies of the in situ formed materials were characterized by SEM. The images of the Co–W film in Figure 2 show small cracks and islands on the surface of the material. A magnified view reveals the fused spheroidal nodules with

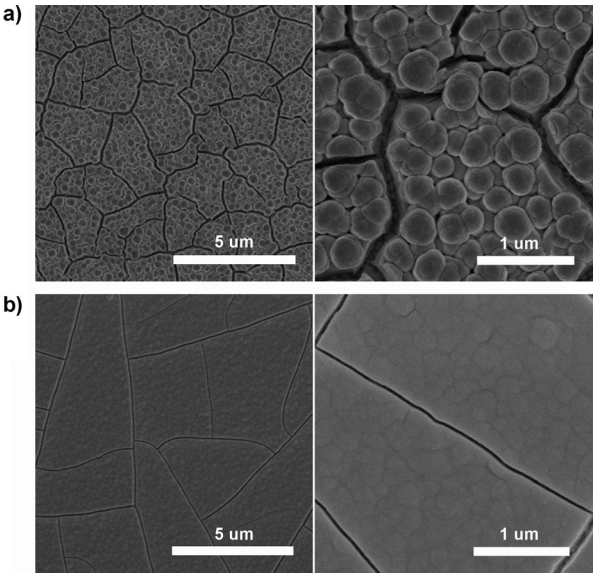

Figure 2. SEM images of a) the Co–W film formed by electrolysis of a 50 mM solution of Na_2WO_4 at pH 8.0 containing 2 mM $Co(NO_3)_2$ for 30 min, and b) the Co–Mo film formed by electrolysis of a 60 mM solution of Na_2MoO_4 at pH 7.6 containing 2 mM $Co(NO_3)_2$ for 30 min.

a size of hundreds of nanometers on the top of these islands. In comparison, the Co–Mo film is more compact and smooth than the Co–W film. The rough structure of the Co–W film provides a larger specific area, which is expected to facilitate oxygen evolution. Additionally, powder XRD patterns also reveal the amorphous character of the Co–W and Co–Mo films (Figure S3 in the Supporting Information).

With no detectable crystallites, the composition of the Co–W and Co–Mo films were assayed by energy-dispersive X-ray analysis (EDX). To eliminate interference from the FTO substrate, the films were scraped off for EDX testing. The EDX spectra in Figure S4 in the Supporting Information show the presence of cobalt, tungsten, and sodium in a ratio of 1:0.44:0.23 for the Co–W film and cobalt, molybdenum, and sodium in a ratio of 1:0.61:0.3 for the Co–Mo film. The ratios of cobalt/tungsten and cobalt/molybdenum were further analyzed by inductively coupled plasma optical emission spectroscopy (ICP-OES) to be 1:0.48 and 1:0.41, respectively. Because tungsten and molybdenum appear to be minor components in the thin film, the structures of the Co–W and Co–Mo film

electrocatalysts were proposed to be dominated by CoO_x.[19,26,27] The Co–W and Co–Mo films on FTO were further analyzed by X-ray photoelectron spectroscopy (XPS). The Co 2p binding energy peaks centered at 780.1 and 795.1 eV for the Co–W film and at 780.4 and 795.5 eV for the Co–Mo film were consistent with Co^{2+} or Co^{3+} bound to oxygen (Figure 3).[16] Oxygen was detected at multiple O 1s binding

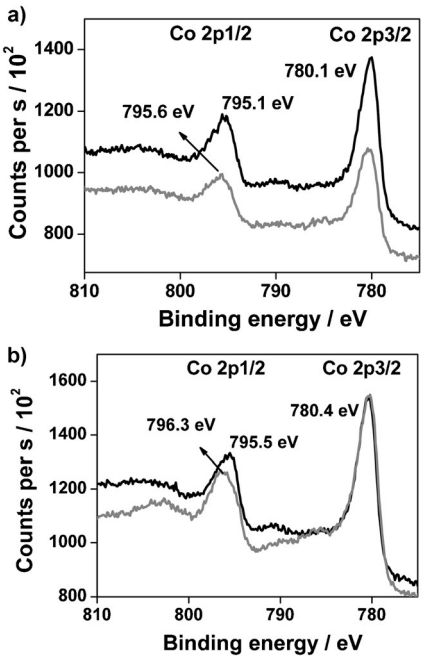

Figure 3. Co 2p XPS spectra of a) as-deposited Co–W film (black) and the Co–W film after 2 h of electrolysis at 1.87 V in a 50 mM aqueous solution of Na_2WO_4 at pH 8.0 (gray); b) as-deposited Co–Mo film (black) and the Co–Mo film after 2 h of electrolysis at 1.85 V in a 60 mM aqueous solution of Na_2MoO_4 at pH 7.6 (gray).

energies, showing a peak at 531.4 eV and a shoulder at 530.3 eV for the Co–W film, and a peak at 531.6 eV and a shoulder at 530.3 eV for the Co–Mo film. The peaks at 531.4 eV and 531.6 eV are consistent with the binding energy of hydroxide species (531–532 eV), whereas the shoulders are consistent with the formation of metal oxides (528–531 eV; Figure S5a and b in the Supporting Information).[16] Finally, the W 4f peaks were observed at 34.4 and 36.7 eV, and the Mo 3d peaks were found at 231.9 and 235.1 eV (Figure S5c and d in the Supporting Information).

In view of practical uses, the activities of the in situ formed electrocatalysts were investigated in aqueous solutions in the absence of Co^{2+}. The experiments were carried out with Co–X (X = W or Mo) deposited on FTO as the working electrode in the three-electrode setup described above. Either a 50 mM solution of Na_2WO_4 at pH 8.0 or a 60 mM solution of Na_2MoO_4 at pH 7.6 was used as the electrolyte. When setting a constant applied potential of 1.87 V for Co–W and 1.85 V for Co–Mo, both oxygen and hydrogen bubbles were immediately released from the working and counter electrodes, respectively. Meanwhile, sustained current densities of 1.45 mA cm^{-2} for FTO/Co–W and 0.95 mA cm^{-2} for FTO/Co–Mo were obtained

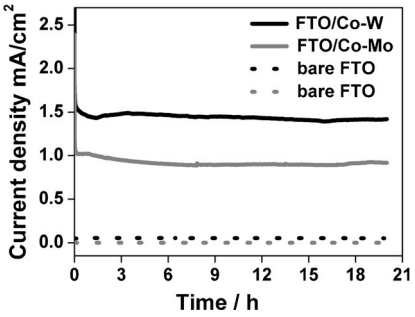

Figure 4. Current density traces for bulk electrolysis at 1.87 V in a 50 mM aqueous solution of Na_2WO_4 at pH 8.0 for the Co–W film (black) and at 1.85 V in a 60 mM aqueous solution of Na_2MoO_4 at pH 7.6 for the Co–Mo film (gray). The electrolysis of bare FTO in solutions of Na_2WO_4 and Na_2MoO_4 are shown as black and gray dotted lines, respectively.

(Figure 4). The turnover frequencies (TOFs) of current system were evaluated based on the assumption that all cobalt atoms in the materials were catalytically active.[28] At an overpotential of 640 mV, TOFs for the Co–W and Co–Mo films were about 0.01 and 0.008 s^{-1}, respectively. The BET surface areas of the catalysts were measured by nitrogen adsorption by using the single-point method.[29] The electrochemical surface area (roughness factor, R_f) of the electrodes was measured from double-layer capacitance measurements (Figure S6 in the Supporting Information).[15,29,30] The specific activities based on either the surface area or R_f of the electrode are given in Table S1 in the Supporting Information.[29] As expected, the catalytic activity increased with the active surface area of the electrode. When a stainless-steel mesh (SSM) was used as a substrate to increase the surface area available for water oxidation, the current density reached 4.5 mA cm^{-2} for the Co–W film (Figure S7 in the Supporting Information).

The long-term stability of a catalyst is a major concern in water splitting. To our delight, no noticeable decay of the anodic currents was observed (less than 5%, Figure 4) during a prolonged period of water electrolysis for 20 h. Under the same applied potential of 1.87 V, the stability of the Co–W catalyst was compared with that of the Co–Pi catalyst deposited on FTO. For comparison, a 50 mM aqueous solution of phosphate buffer at pH 8 was used for the Co–Pi system as the electrolyte. As shown in Figure 5, a high current density of

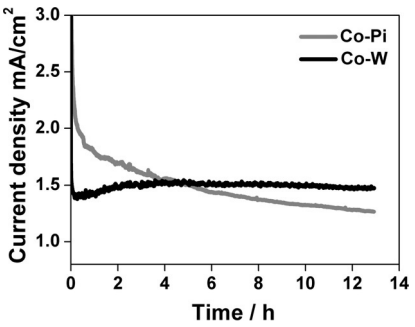

Figure 5. CPE of water at 1.87 V in a 50 mM aqueous solution of Na_2WO_4 at pH 8.0 for the FTO/Co–W electrode and at 1.85 V in a 50 mM aqueous solution of KPi at pH 8.0 for the FTO/Co–Pi electrode.

2.0 mA cm^{-2} was acquired for Co–Pi at the beginning of electrolysis, which dropped to 1.26 mA cm^{-2} over 13 h and corresponded to a 37% decay in activity. This is in sharp contrast to the Co–W system, which maintains a stable current at a level of 1.5 mA cm^{-2}. In addition to Co–Ci, this is another example of a cobalt-based electrocatalyst showing long-term stability in a cobalt-free electrolyte solution under benign conditions.[25]

The proton-accepting electrolyte is essential to the catalytic activity. Electrolysis proceeded in a solution of Na_2SO_4, which showed that both electrodes lost activity rapidly (Figure S8 in the Supporting Information). Furthermore, electrolysis with the Co–W and Co–Mo films was performed in 0.1 M KPi buffer at pH 8. At 1.87 V, the current densities for both films stabilized at 1.0 mA cm^{-2} over 10 h (Figure S9 in the Supporting Information). In 0.1 M KBi buffer at pH 9, the Co–W and Co–Mo films also exhibited similar activities, although these were lower than that in KPi (Figure S10 in the Supporting Information). These results suggest that the main structures of the Co–W and Co–Mo catalysts are similar, and their catalytic activities depend on the type of proton-accepting electrolyte.

To further explore the properties of two cobalt oxide modified electrodes, the current densities of the Co–W and Co–Mo catalysts on FTO were measured as a function of overpotential (Figure S11 in the Supporting Information). Observable catalytic currents start at $\eta = 210$ mV for Co–W and at $\eta = 280$ mV for Co–Mo at pH 8. For a catalytic current of 1 mA cm^{-2}, the required overpotentials are $\eta = 420$ mV for Co–W and $\eta = 500$ mV for Co–Mo. Compared with the other electrocatalysts based on non-noble-metal oxides under benign conditions reported in Table 1, Co–W showed a lower onset potential and higher catalytic activity for water oxidation.[32–38] Tafel slopes of Co–W and Co–Mo were determined to be 133 and 79 mV dec^{-1}, respectively (Figure 6a). The different Tafel slopes might be attributed to different catalytic mechanisms exerted by the Co–W and Co–Mo films. The pH dependence of the steady-state current was explored at an applied potential of 1.1 V versus Ag/AgCl (Figure 6b). The log(j)–pH curve of Co–W at a constant potential exhibits a liner dependence on the pH in the range of 5.3 to 8.2, although higher pH values have little effect on the current density. Similarly, the current density of the FTO/Co–Mo electrode increases along with pH from pH 4.3 to pH 6. The log(j)–pH curve flattens out beyond pH 6. These results might be due to changes in the mechanism, probably associated with deprotonated intermediates.[17]

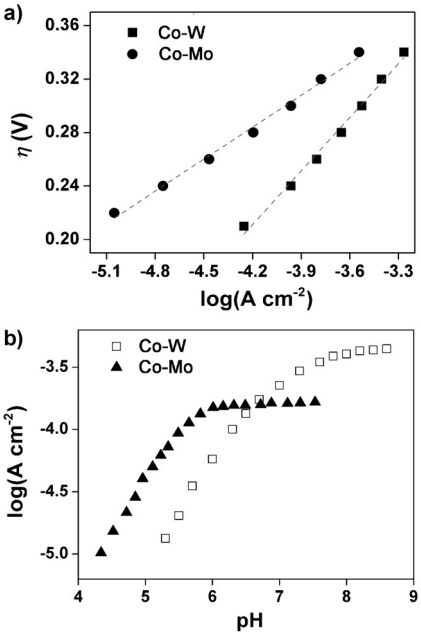

Figure 6. a) Tafel plots, $\eta = (V_{appl} - iR) - E_{pH}$ (in which V_{appl} is the applied potential), of the Co–W film in 50 mM Na_2WO_4 electrolyte at pH 8.0, and the Co–Mo film in 60 mM Na_2MoO_4 electrolyte, pH 7.6, corrected for the iR drop of the solutions. b) Current density dependence on pH in 50 mM Na_2WO_4 electrolyte for the Co–W film and in 60 mM Na_2MoO_4 electrolyte for the Co–Mo film. The potential was set at 1.1 V versus Ag/AgCl, with no iR compensation.

Table 1. A comparison of some catalytic parameters for non-noble-metal oxide water oxidation catalysts.[31]

Catalyst	$\eta^{[a]}$ [mV]	$\eta^{[b]}$ [mV]	Tafel slope [mV dec^{-1}]	pH	Ref.
MnO_x	<300	>1000	127	8.5–5.5	[33]
CoO_x	<200	<300	65	7	[24]
MnO_x	390	590	60–80	7	[38]
MnO_x	441	600	120	7	[34]
CoFePBA[c]	291	>600	88	7	[36]
MnO_x	150	>1000	–	7	[37]
CoPi	281	410	60	7	[17]
$Co(PO_3)_2$	310	320	74	6.4	[15]
MnO_x	>700	>1000	109	7	[32]
$Li_xMnP_2O_7$	500	–	120	7	[35]
Co–W	210	420	133	8	this work
Co–Mo	280	500	79	7.6	this work

[a] Onset overpotential. [b] Overpotential for 1 mA cm^{-2}. [c] PBA = Prussian blue analogue.

In a separate experiment, oxygen evolved at 1.87 V for 5 h was detected online by means of a fluorescence-based oxygen sensor fixed in the headspace of a gas-tight electrolytic cell and quantified by GC (Figures S12 and S13 in the Supporting Information). The amount of oxygen produced was determined to be 48.9 μmol for the Co–W catalyst, which well matched with the 19.14 C of charge passed during electrolysis, and was consistent with nearly quantitative Faradaic efficiency (Figure 7a). For the FTO/Co–Mo electrode, the Faradaic efficiency was determined to be 98% (Figure 7b).

The Co–W and Co–Mo films were analyzed by SEM, EDX, and XPS after electrolysis for a period of 2 h. No clear change could be observed from the SEM images (Figure S14 in the Supporting Information). The ratio of cobalt/tungsten/sodium in the Co–W film and the ratio of cobalt/molybdenum/sodium in the Co–Mo film remained constant throughout electrolysis (Figure S15 in the Supporting Information). The XPS spectra showed no shift in the W 4f and Mo 3d peaks after electrolysis; this was indicative that there were no

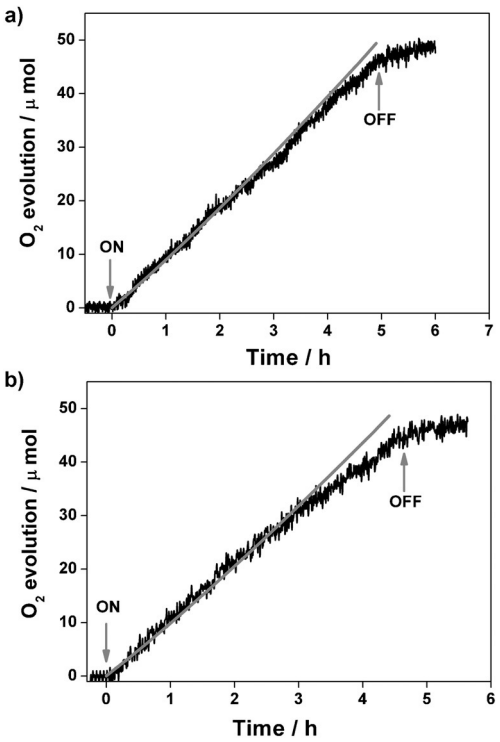

Figure 7. Determination of the Faradaic efficiency of the FTO/Co–W film at 1.87 V in a 50 mM aqueous solution of Na_2WO_4 at pH 8.0 (a), and the FTO/Co–Mo film at 1.85 V in a 60 mM aqueous solution of Na_2MoO_4 at pH 7.6 (b). Gray line: theoretical amount of oxygen assumed for the passed charge with 100% Faradaic efficiency. Black line: the amount of oxygen measured by the oxygen sensor.

valence changes on tungsten and molybdenum (Figure S5 c and d in the Supporting Information). However, the shift of the Co 2p binding energy peak from 795.1 to 795.6 eV for the Co–W film, and from 795.5 to 796.3 eV for the Co–Mo film, indicated an increase in the cobalt oxidation state. This was further evidenced by the enhanced binding energy of O 1s at 530.3 eV, which was associated with the formation of cobalt with a higher oxidation state (Figure S5 a and b in the Supporting Information).[16] Therefore, we proposed a similar reaction mechanism for our system to that of the Co–Pi system, in which multiple proton-coupled electron transfer processes were involved in the oxidation of water and the key step was the proton-coupled one-electron conversion of Co^{III}–OH into Co^{IV}–O, prior to oxygen evolution.[39–42]

Conclusion

We have shown efficient electrochemical water oxidation under benign conditions by using amorphous cobalt oxide catalysts generated in situ from Co^{2+} in aqueous solutions of tungstate and molybdate. The Co–W and Co–Mo films as robust catalytic materials are not only the surrogates of Co–Pi, but also show excellent stability in cobalt-free aqueous solutions.

Experimental Section

Materials

FTO substrates were purchased from Dalian Heptachroma Solar-Tech Co., Ltd., (thickness ≈2.2 mm, transmittance >90%, resistance ≈50 mΩ cm^{-2}). All other chemicals for the preparation of Co–W and Co–Mo films were commercially available, and all solvents were of reagent grade and dried prior to use according to standard methods.

Instruments

Electrochemical measurements were performed with a CHI660D electrochemical potentiostat. SEM micrographs and EDX analyses were performed on a Nova NanoSEM 450 instrument with an accelerating voltage of 10.0 kV. XRD results were collected with a D/max-2400 diffractometer. XPS was performed on an ESCALAB250 instrument (Thermo VG company, USA). Nitrogen adsorption isotherms were obtained by using a Quantachrome AUTOSORB-1-MP instrument at 77 K. ICP-OES was performed on a PerkinElmer Optima 2000 DV instrument.

Fabrication of Catalyst Films

In a typical experiment, a three-electrode cell equipped with the FTO electrode as the working electrode, Pt net as the counter electrode, and a reference electrode of Ag/AgCl in an aqueous solution of KCl (3.5 M) was used for electrodeposition at 1.87 V (vs. RHE) for 30 min. The electrolyte was prepared as outlined below. For the Co–W film, $Co(NO_3)_2{\cdot}6H_2O$ (11.6 mg) in water (0.2 mL) was added dropwise to a 50 mM solution of Na_2WO_4 at pH 8.0 (20 mL) under stirring. For the Co–Mo film, $Co(NO_3)_2{\cdot}6H_2O$ (11.6 mg) in water (0.2 mL) was added dropwise to a 60 mM solution of Na_2MoO_4 at pH 7.6 (20 mL) under stirring.

Electrochemical Measurements

Electrochemical experiments were run in a three-electrode single-compartment cell. The cell was equipped with the FTO/Co–W or FTO/Co–Mo electrodes as the working electrode, a Pt wire as the counter electrode, and an Ag/AgCl (3.5 M KCl in water) reference electrode. CV and long-term controlled-potential electrolysis without stirring were carried out in a solution of Na_2WO_4 at pH 8 for the FTO/Co–W electrode and in a solution of Na_2MoO_4 at pH 7.6 for the FTO/Co–Mo electrode at ambient pressure and room temperature.

The roughness factors (R_f) of the electrodes were determined based on the double-layer charging curves by using CV within a small potential range (0.94 to 1.04 V vs. RHE). The double-layer capacitance values were determined from the slope of the capacitive current versus the scan rate, which were further divided by the value of 60 μF cm^{-2} to obtain R_f.

To determine the Faradaic efficiency, the electrolysis cell was sealed and purged with argon. An Ocean Optics oxygen sensor (FOXY-OR125-G) attached to a multifrequency phase fluorometer (MFPF-100) was fixed in the headspace of the cell (Figure S12 in the Supporting Information). The kinetics of O_2 evolution were recorded by the oxygen sensor during electrolysis of the degassed electrolyte solutions. Upon terminating electrolysis, the O_2 signal was recorded for an additional 1 h and the actual quantity of O_2 was determined by using a GC 7890T instrument equipped with a thermal conductive detector. The theoretical amount of oxygen produced was obtained by converting the charge passed into mi-

cromoles of gas according to Faraday's Law. The Faradaic efficiency was calculated as $O_{2(actual)}/O_{2(theoretical)} \times 100\%$.

Acknowledgements

This work was supported by the National Natural Science Foundation of China (21476043, 21120102036, and 21361130020), the National Basic Research Program of China (973 program) (2014CB239402) and the Fundamental Research Funds for the Central Universities (DUT14YQ104).

Keywords: cobalt · heterogeneous catalysis · molybdenum · tungsten · water splitting

[1] N. S. Lewis, D. G. Nocera, *Proc. Natl. Acad. Sci. USA* **2006**, *103*, 15729 – 15735.
[2] A. J. Bard, M. A. Fox, *Acc. Chem. Res.* **1995**, *28*, 141 – 145.
[3] S. Y. Reece, J. A. Hamel, K. Sung, T. D. Jarvi, A. J. Esswein, J. J. Pijpers, D. G. Nocera, *Science* **2011**, *334*, 645 – 648.
[4] K. S. Joya, Y. F. Joya, K. Ocakoglu, R. van de Krol, *Angew. Chem. Int. Ed.* **2013**, *52*, 10426 – 10437; *Angew. Chem.* **2013**, *125*, 10618 – 10630.
[5] T. W. Kim, K. S. Choi, *Science* **2014**, *343*, 990 – 994.
[6] K. S. Joya, H. J. de Groot, *ChemSusChem* **2014**, *7*, 73 – 76.
[7] T. J. Meyer, *Nature* **2008**, *451*, 778 – 779.
[8] K. S. Joya, J. L. Vallés-Pardo, Y. F. Joya, T. Eisenmayer, B. Thomas, F. Buda, H. J. M. de Groot, *ChemPlusChem* **2013**, *78*, 35 – 47.
[9] H. Yamazaki, A. Shouji, M. Kajita, M. Yagi, *Coord. Chem. Rev.* **2010**, *254*, 2483 – 2491.
[10] D. Seley, K. Ayers, B. A. Parkinson, *ACS Comb. Sci.* **2013**, *15*, 82 – 89.
[11] T. Nakagawa, N. S. Bjorge, R. W. Murray, *J. Am. Chem. Soc.* **2009**, *131*, 15578 – 15579.
[12] Y. H. Fang, Z. P. Liu, *J. Am. Chem. Soc.* **2010**, *132*, 18214 – 18222.
[13] R. D. Smith, M. S. Prevot, R. D. Fagan, S. Trudel, C. P. Berlinguette, *J. Am. Chem. Soc.* **2013**, *135*, 11580 – 11586.
[14] R. D. Smith, M. S. Prévot, R. D. Fagan, Z. Zhang, P. A. Sedach, M. K. J. Siu, S. Trudel, C. P. Berlinguette, *Science* **2013**, *340*, 60 – 63.
[15] H. S. Ahn, T. D. Tilley, *Adv. Funct. Mater.* **2013**, *23*, 227 – 233.
[16] J. B. Gerken, E. C. Landis, R. J. Hamers, S. S. Stahl, *ChemSusChem* **2010**, *3*, 1176 – 1179.
[17] M. W. Kanan, D. G. Nocera, *Science* **2008**, *321*, 1072 – 1075.
[18] B. S. Yeo, A. T. Bell, *J. Am. Chem. Soc.* **2011**, *133*, 5587 – 5593.
[19] D. K. Bediako, B. Lassalle-Kaiser, Y. Surendranath, J. Yano, V. K. Yachandra, D. G. Nocera, *J. Am. Chem. Soc.* **2012**, *134*, 6801 – 6809.
[20] K. S. Joya, Y. F. Joya, H. J. M. de Groot, *Adv. Energy Mater.* **2014**, *4*, 1301929.
[21] A. Singh, S. L. Y. Chang, R. K. Hocking, U. Bach, L. Spiccia, *Energy Environ. Sci.* **2013**, *6*, 579 – 586.
[22] S. M. Barnett, K. I. Goldberg, J. M. Mayer, *Nat. Chem.* **2012**, *4*, 498 – 502.
[23] M. T. Zhang, Z. Chen, P. Kang, T. J. Meyer, *J. Am. Chem. Soc.* **2013**, *135*, 2048 – 2051.
[24] J. B. Gerken, J. G. McAlpin, J. Y. Chen, M. L. Rigsby, W. H. Casey, R. D. Britt, S. S. Stahl, *J. Am. Chem. Soc.* **2011**, *133*, 14431 – 14442.
[25] K. S. Joya, K. Takanabe, H. J. M. de Groot, *Adv. Energy Mater.* **2014**, *4*, 1400252.
[26] D. K. Bediako, Y. Surendranath, D. G. Nocera, *J. Am. Chem. Soc.* **2013**, *135*, 3662 – 3674.
[27] P. Du, O. Kokhan, K. W. Chapman, P. J. Chupas, D. M. Tiede, *J. Am. Chem. Soc.* **2012**, *134*, 11096 – 11099.
[28] L. Trotochaud, J. K. Ranney, K. N. Williams, S. W. Boettcher, *J. Am. Chem. Soc.* **2012**, *134*, 17253 – 17261.
[29] X. Liu, Z. Chang, L. Luo, T. Xu, X. Lei, J. Liu, X. Sun, *Chem. Mater.* **2014**, *26*, 1889 – 1895.
[30] J. Kibsgaard, T. F. Jaramillo, *Angew. Chem. Int. Ed.* **2014**, *53*, 14433 – 14437; *Angew. Chem.* **2014**, *126*, 14661 – 14665.
[31] J. R. Galán-Mascarós, *ChemElectroChem* **2015**, *2*, 37 – 50.
[32] A. Bergmann, I. Zaharieva, H. Dau, P. Strasser, *Energy Environ. Sci.* **2013**, *6*, 2745 – 2755.
[33] M. Huynh, D. K. Bediako, D. G. Nocera, *J. Am. Chem. Soc.* **2014**, *136*, 6002 – 6010.
[34] A. Indra, P. W. Menezes, I. Zaharieva, E. Baktash, J. Pfrommer, M. Schwarze, H. Dau, M. Driess, *Angew. Chem. Int. Ed.* **2013**, *52*, 13206 – 13210; *Angew. Chem.* **2013**, *125*, 13447 – 13451.
[35] J. Park, H. Kim, K. Jin, B. J. Lee, Y. S. Park, H. Kim, I. Park, K. D. Yang, H. Y. Jeong, J. Kim, K. T. Hong, H. W. Jang, K. Kang, K. T. Nam, *J. Am. Chem. Soc.* **2014**, *136*, 4201 – 4211.
[36] S. Pintado, S. Goberna-Ferron, E. C. Escudero-Adan, J. R. Galan-Mascaros, *J. Am. Chem. Soc.* **2013**, *135*, 13270 – 13273.
[37] A. Singh, R. K. Hocking, S. L. Y. Chang, B. M. George, M. Fehr, K. Lips, A. Schnegg, L. Spiccia, *Chem. Mater.* **2013**, *25*, 1098 – 1108.
[38] I. Zaharieva, P. Chernev, M. Risch, K. Klingan, M. Kohlhoff, A. Fischer, H. Dau, *Energy Environ. Sci.* **2012**, *5*, 7081 – 7089.
[39] Y. Surendranath, D. K. Bediako, D. G. Nocera, *Proc. Natl. Acad. Sci. USA* **2012**, *109*, 15617 – 15621.
[40] Y. Surendranath, M. W. Kanan, D. G. Nocera, *J. Am. Chem. Soc.* **2010**, *132*, 16501 – 16509.
[41] M. Zhang, M. d. Respinis, H. Frei, *Nat. Chem.* **2014**, *6*, 362 – 367.
[42] M. Grzelczak, J. Zhang, J. Pfrommer, J. Hartmann, M. Driess, M. Antonietti, X. Wang, *ACS Catal.* **2013**, *3*, 383 – 388.

Manuscript received: January 28, 2015
Final Article published: April 29, 2015